Perturbative QCD predictions for inclusive production of heavy mesons in e^+e^- annihilation

Chueng-Ryong Ji*
Stanford Linear Accelerator Center, Stanford University, Stanford, California 94305
and Institute of Theoretical Physics, Department of Physics, Stanford University, Stanford, California 94305

Farhang Amiri†
Stanford Linear Accelerator Center, Stanford University, Stanford, California 94305
(Received 18 August 1986)

Within the framework of a particular model for meson production, we have performed a perturbative QCD analysis for inclusive production of heavy mesons D, B, and T at an energy range of 20—110 GeV. At the high-energy limit, analytic calculations of total cross sections, fragmentation functions, and angular distributions are presented. For T mesons, all mass terms in the leading-order perturbative calculation are included in numerical estimates. We found these terms give 20—30% corrections for D- and B-meson production at $\sqrt{s} \sim 60$ GeV. The forward-backward asymmetry from weak-electromagnetic interference is found to be large at KEK TRISTAN energy.

I. INTRODUCTION

The present vigorous experimental programs at the existing accelerators and at the ones under construction are expected to subject quantum chromodynamics (QCD) and electroweak theory to ever more stringent tests. Specifically, e^+e^- colliders at center-of-mass energies of $\sqrt{s} \sim 100$ GeV will provide the opportunity to explore many of the predictions of QCD and electroweak theory in a clean environment and therefore they are ideal testing grounds within their energy ranges.

In e^+e^- annihilations, the interaction is mediated by electromagnetic current (γ) and the weak neutral current (Z^0) (Ref. 1). At typical operating energies of the Stanford Linear Collider[2] and CERN LEP,[3] the interaction will be dominated through a neutral current via Z^0 production. Furthermore, large enhancements in the value of the cross section for $e^+e^- \rightarrow$hadrons is expected at a Z^0 resonance, i.e., at a c.m. total energy of $\sqrt{s} \sim M_Z$. However, at lower energies (i.e., $\sqrt{s} \sim 20$ GeV), the process is dominated by electromagnetic current and Z^0 contribution will be negligible. The interesting region of medium energy [e.g., KEK TRISTAN (Ref. 4) energies] will reveal the interference between weak and electromagnetic interactions.

Related to the variation of energy in inclusive hadron production, it is interesting to study the angular distribution of produced hadrons. At energies slightly above threshold, the reaction is almost like a two-body exclusive process. Therefore, the angular distribution is determined by the helicity of the final-state hadrons. However, at higher energies, multiparticle production dominates and the spin correlations among produced hadrons become unimportant. In fact, at asymptotic high energies, the angular distribution of the hadron in inclusive reaction is basically determined by the quark-antiquark pair production.

Another interesting feature of angular distribution of hadrons come from weak and electromagnetic interference.[1] The axial-vector coupling of the Z^0 boson to fermions gives rise to asymmetry in the angular distribution. This leads to forward-backward asymmetry which can provide valuable information about the coupling of Z^0 to quarks.

In this paper, we have studied the inclusive production of heavy mesons (mesons with at least one heavy quark c,b,t) for the energy ranges from 20 GeV to 110 GeV. From a theoretical point of view, heavy-meson systems are interesting because (i) their binding energies are small compared to their masses and therefore to a good approximation they are nonrelativistic systems described by simple wave functions (see Sec. II) and (ii) the momentum transfer q involved in the production of heavy quarks is sufficiently large compared to QCD scale parameter $\Lambda_{\rm QCD} \sim 100$ MeV. Thus, the heavy-meson system could provide important clues related to the perturbative QCD mechanism for the hadronization process.[5] The proposed mechanism we adopted in this study is the one-gluon-exchange process as will be explained in the next section.

This paper is organized as follows. In Sec. II, we present the details of the calculation for production of heavy mesons. We derive analytic expressions for various cross sections at the high-energy limit in Sec. III. The numerical estimates of total cross section, fragmentation function, angular distribution and asymmetry for pseudoscalar mesons are given in Sec. IV, followed by a summary and conclusions in Sec. V.

II. CALCULATION OF CROSS SECTION

Our calculation is based on a particular model for meson production.[6] We include explicit effects associated with the meson bound state by assuming that in the low-momentum transfer domain, the meson wave function de-

scribes a quark-antiquark bound state and that at large momentum transfer the momentum dependence of the meson wave function is controlled by the Bethe-Salpeter kernel and thus by single-gluon exchange in the asymptotic limit. The mechanism based on this idea for inclusive production of heavy mesons is shown in Fig. 1. In Figs. 1(a) and 1(b), the process is mediated via photon production while in Figs. 1(c) and 1(d) it is mediated through the Z^0 boson. The main contribution from each set of diagrams depends on the energy regions, as was discussed in the Introduction.

In this model, the invariant amplitude $\mathcal{M}$ at large momentum transfer q for processes shown in Fig. 1 factorizes[5–7] into the convolution of hard-scattering amplitude T_H and meson-distribution amplitude ϕ_M. A necessary (but not sufficient) condition for the factorization is illustrated in the Appendix. Therefore, we can write $\mathcal{M}$ as

$$\mathcal{M}(k_i,q_i)=\int [dx]T_H(k_i,q_i,x_i)\phi_M(x_i,q^2)\ , \tag{1}$$

where T_H is the hard-scattering amplitude which can be calculated perturbatively from quark-gluon subprocesses, and ϕ_M is the probability amplitude to find quarks which are collinear up to the scale q^2 in a mesonic bound state. In Eq. (1), x_i's are the momentum fractions carried by constituent quarks and $[dx]=dx_1dx_2\delta(1-x_1-x_2)$. For the heavy-quark system, we use the bound-state wave function determined by nonrelativistic considerations as a further model assumption. The use of a nonrelativistic wave function is probably not realistic, especially for mesons in which the lighter-quark mass is comparable to the binding energy. However, it serves as a useful guide and one eventually hopes to use the actual distribution amplitudes when they become available. For now, we use the quark distribution amplitude ϕ_M, given in Ref. 7, which is derived in nonrelativistic approximation.[7] For pseudoscalar mesons, ϕ_M is given by

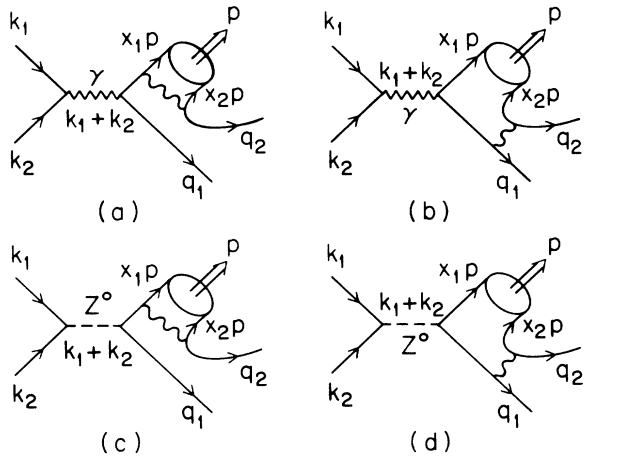

FIG. 1. Inclusive production of mesons in e^+e^- annihilations. Four more diagrams can be obtained by exchanging primary- and secondary-quark pairs.

$$\phi_M(x_i,q^2)=\frac{f_M}{2\sqrt{3}}\delta\left[x_1-\frac{m_1}{m}\right]\ , \tag{2}$$

where f_M is the pseudoscalar-meson decay constant and m and m_1 are masses of the meson and the primary quark, respectively. By substituting Eq. (2) into Eq. (1), the invariant amplitude $\mathcal{M}$ becomes

$$\mathcal{M}(k_i,q_i)=\frac{f_M}{2\sqrt{3}}T_H(k_i,q_i,r)\ , \tag{3}$$

where $r=m_1/m$. Using the spin sum[8]

$$\frac{1}{\sqrt{2}}\sum_{\text{spin}}v(p)\bar{u}(p)=\frac{\gamma_5(\not{p}+m)}{\sqrt{2}} \tag{4}$$

for pseudoscalar mesons, the hard-scattering amplitude T_H can be expressed as

$$\begin{aligned}T_H=\sum_{I=\gamma,Z^0} & i\frac{16\pi^2C_F\alpha\alpha_s}{(1-r)s(\sqrt{s}-2E_1)s_I}\bar{v}(k_2)\gamma^\mu\Gamma_e^I u(k_1)\\ &\times\left[\frac{\bar{u}(q_2)\gamma_\alpha\dfrac{\gamma_5(\not{p}+m)}{\sqrt{2}}\gamma^\alpha(\not{p}+\not{q}_2+rm)\gamma_\mu\Gamma_Q^I v(q_1)}{\sqrt{s}-2E_1}\right.\\ &\left.+\frac{\bar{u}(q_2)\gamma_\alpha\dfrac{\gamma_5(\not{p}+m)}{\sqrt{2}}\gamma_\mu\Gamma_Q^I\{-[\not{q}_1+\not{q}_2+(1-r)\not{p}]+rm\}\gamma^\alpha v(q_1)}{\sqrt{s}-2rE}\right]+(\text{primary}\leftrightarrow\text{secondary})\ ,\end{aligned} \tag{5}$$

where

$$\begin{aligned}&s_\gamma=s,\quad s_{Z^0}=4\sin^2\!2\theta_W(s-M_Z{}^2+i\Gamma_ZM_Z)\ ,\\ &\Gamma_e^\gamma=-1,\quad \Gamma_e^Z=V_e+A_e\gamma_5\ ,\\ &\Gamma_Q^\gamma=Q,\quad \Gamma_Q^Z=V_Q+A_Q\gamma_5\ ,\end{aligned} \tag{6}$$

with

$$\begin{aligned}&V_Q=2I_3-4Q\sin^2\theta_W,\quad V_e=4\sin^2\theta_W-1\\ &A_Q=-2I_3,\quad A_e=1\ .\end{aligned} \tag{7}$$

Here I_3 is the third component of the weak isospin of the

quark coupled to Z^0 and Q is the charge of the quark. In Eq. (5), α is the fine-structure constant, the color factor $C_F=\frac{4}{3}$, E and E_1 are energies of the meson and the primary quark, respectively, and (primary↔secondary) indicates the contributions from the diagrams in which the primary-quark pair is exchanged with the secondary-quark pair.

Now the square of the invariant amplitude $\mathscr{M}$ becomes

$$|\mathscr{M}|^2=\frac{f_M{}^2}{12}\frac{128\pi^4 C_F{}^2\alpha^2\alpha_s{}^2}{(1-r)^2 s^2(\sqrt{s}-2E_1)^2}\times\sum_{I,J}^{\gamma,Z^0}\frac{1}{s_I s_J^*}L^{\mu\nu}(I,J)H_{\mu\nu}(I,J)\ , \tag{8}$$

where

$$L^{\mu\nu}(I,J)=\mathrm{Tr}(k_2\gamma^\mu\Gamma_e^I k_1\tilde{\Gamma}_e^J\gamma^\nu) \tag{9}$$

and

$$\begin{aligned}H_{\mu\nu}(I,J)=&-\frac{4}{(\sqrt{s}-2E_1)^2}\mathrm{Tr}\{[q_2+(1-r)m]\gamma_5(\not p-2m)(\not p+\not q_2+rm)\gamma_\mu\Gamma_Q^I(\not q_1-rm)\tilde{\Gamma}_Q^J\gamma_\nu(\not p+\not q_2+rm)(\not p-2m)\gamma_5\}\\&+\frac{4}{(\sqrt{s}-2E_1)(\sqrt{s}-2rE)}\mathrm{Re}\{\mathrm{Tr}\{[q_2+(1-r)m]\gamma_5(\not p-2m)(\not p+\not q_2+rm)\gamma_\mu\Gamma_Q^I(\not q_1-rm)\\&\times\gamma^\alpha[\not q_1+\not q_2+(1-r)\not p-rm]\tilde{\Gamma}_Q^J\gamma_\nu(\not p+m)\gamma_5\gamma_\alpha\}\}\\&-\frac{1}{(\sqrt{s}-2rE)^2}\mathrm{Tr}\{[q_2+(1-r)m]\gamma_\alpha\gamma_5(\not p+m)\gamma_\mu\Gamma_Q^I[\not q_1+\not q_2+(1-r)\not p-rm]\gamma^\alpha(\not q_1-rm)\\&\times\gamma^\beta[\not q_1+\not q_2+(1-r)\not p-rm]\tilde{\Gamma}_Q^J\gamma_\nu(\not p+m)\gamma_5\gamma_\beta\}\ .\end{aligned} \tag{10}$$

In Eqs. (9) and (10), $\tilde{\Gamma}_a\equiv V_a-\gamma_5 A_a$. Using Eqs. (8)—(10), we can calculate the differential cross section for the process $e^+e^-\to\text{meson}+X$:

$$d\sigma=\frac{|\overline{\mathscr{M}}|^2}{2s}\frac{d^3P}{2E}\frac{d^3q_1}{2E_1}\frac{d^3q_2}{2E_2}\frac{1}{(2\pi)^5}\times\delta^4(k_1+k_2-p-q_1-q_2)\ , \tag{11}$$

where $|\overline{\mathscr{M}}|^2$ is the square of the spin-averaged invariant amplitude. Utilizing energy-momentum conservation, the differential cross section (11) becomes

$$d\sigma=\frac{|\overline{\mathscr{M}}|^2}{64(2\pi)^5}dz\,dy\,d\cos\theta\,d\phi\,d\cos\theta_{MQ}d\phi_{MQ}\times\delta\left[\cos\theta_{MQ}-\frac{2-2(y+z)+yz+r\tau^2}{(z^2-\tau^2)^{1/2}(y^2-r^2\tau^2)^{1/2}}\right]\times\theta(2-y-z)\ , \tag{12}$$

where $y=2E_1/\sqrt{s}$, $z=2E/\sqrt{s}$, $\tau^2=4m^2/s$, angles (θ,ϕ) specify the direction of the meson with respect to the beam axis, (θ_{MQ},ϕ_{MQ}) determine the direction of the primary quark with respect to the meson, and the function $\theta(2-y-z)$ is theta function. The final form of the differential cross section can be obtained by integrating over $\cos\theta_{MQ}$ and ϕ (integrand is independent of azimuthal angle of the meson). Therefore, we get

$$d\sigma=\frac{|\overline{\mathscr{M}}|^2}{1024\pi^4}dz\,dy\,d\cos\theta d\phi_{MQ}\ . \tag{13}$$

The limits of y integration[5] satisfy the equation $\cos^2\theta_{MQ}=1$, or

$$[4(1-z)+\tau^2]y^2-2(2-z)[2(1-z)+r\tau^2]y+[2(1-z)+r\tau^2]^2+r^2\tau^2(z^2-\tau^2)=0\ . \tag{14}$$

In the following section we will use Eqs. (8)—(13) to determine cross sections for various pseudoscalar mesons.

III. CROSS SECTIONS AT HIGH-ENERGY LIMIT

In this section we derive an analytic expression for the differential cross section of Eq. (13) in the limiting case of $m^2/s\to 0$. This high-energy limit is mainly applicable to the production of D and B mesons at SLC and LEP energies where meson mass can be neglected compared to total c.m. energy.

Let us return to Eq. (14) where its solutions represent the limits of y integration in differential cross section of Eq. (13). If $\tau^2=4m^2/s\ll 1$, then the solutions[5] of Eq. (14) to the first order of τ^2 are

$$\begin{aligned}y_l&=1-z+\frac{[1-(1-r)z]^2}{4z(1-z)}\tau^2\ ,\\ y_u&=1-\frac{[1-(1-r)z]^2}{4z(1-z)}\tau^2\ .\end{aligned} \tag{15}$$

Consequently, by integrating over y and using the limits given by (15), the differential cross section becomes

$$\lim_{\tau^2\to 0}\frac{d\sigma}{dz}=\frac{2\pi\alpha^2\alpha_s^2 f_M{}^2}{27\sin^4 2\theta_W m^2}\frac{s}{(s-M_Z{}^2)^2+\Gamma_Z{}^2M_Z{}^2}\times z(1-z)^2\left[\Gamma_p\frac{[1+(1-r)z]^2}{(1-r)^2(1-rz)^4}+\Gamma_s\frac{(1+rz)^2}{r^2[1-(1-r)z]^4}\right]\ , \tag{16}$$

where

$$\Gamma_{p,s}=\tfrac{1}{3}(V_{p,s}{}^2+V_{Qp,s}{}^2A_e{}^2+A_{Qp,s}{}^2V_e{}^2+A_{Qp,s}{}^2A_e^2) \tag{17}$$

with

$$V_{p,s}=V_{Qp,s}V_e-4Q_{p,s}\sin^2\theta_W\frac{(s-M_Z{}^2)^2+\Gamma_Z{}^2M_Z{}^2}{s^2} . \tag{18}$$

Here $Q_{p,s}$ refer to primary and secondary quark charges. Now we calculate the fragmentation function $D_Q^M(z)$ which is related to the differential cross section by

$$D_Q^M(z)\equiv\frac{1}{\sigma}\frac{d\sigma}{dz} , \tag{19}$$

where σ is the total cross section and is obtained by integrating Eq. (16). The result is

$$\sigma=\frac{2\pi\alpha^2\alpha_s{}^2f_M{}^2}{27\sin^4\theta_W m^2}\frac{s}{(s-M_Z{}^2)^2+\Gamma_Z{}^2M_Z{}^2}\times[\Gamma_p g(r)+\Gamma_s g(1-r)] , \tag{20}$$

where

$$g(r)=\frac{\ln(1-r)}{r^6(1-r)^2}(10-20r+16r^2-6r^3+r^4)+\frac{1}{6r^5(1-r)^3}(60-150r+146r^2-69r^3+15r^4) . \tag{21}$$

Therefore using Eqs. (16) and (20), the fragmentation function defined by (19) becomes

$$D_Q^M(z)=z(1-z)^2\left[\Gamma_p\frac{[1+(1-r)z]^2}{(1-r)^2(1-rz)^4}+\Gamma_s\frac{(1+rz)^2}{r^2[1-(1-r)z]^4}\right]\Big/[\Gamma_p g(r)+\Gamma_s g(1-r)] , \tag{22}$$

where $\Gamma_{p,s}$ is given by Eq. (17).

It is interesting to note that even though experimental data from SLC or LEP are not yet available, but the measurements of fragmentation functions of heavy quarks at SLAC PEP or DESY PETRA indicate $(1-z)^2$ behavior at large-z values, i.e., z close to 1. This is precisely what is predicted by Eq. (22). Furthermore, at r values near 1 (but not exactly 1), e.g., for D and B mesons, the contributions from the secondary-quark pair (light-quark—antiquark pair) in Eqs. (16) and (20) become negligible and we get

$$D_Q^M(z)\approx\frac{1}{g(r)}\frac{[1+(1-rz)]^2}{(1-r)^2(1-rz)^4}z(1-z)^2 , \tag{23}$$

where $g(r)$ is given by (21). Therefore, the coefficient Γ_p which contains the information about the coupling of Z^0 to quarks and leptons cancels and the fragmentation function becomes exactly what was calculated in Ref. 5 based on only photon exchange. One can easily see that Eq. (23) has the z dependence

$$D(z)\propto\frac{(1-r)z(1-z)^2}{(1-rz)^4}$$

if r is close to 1. This becomes $\delta(1-z)$ when $r=1$ and has $1/(1-z)^2$ behavior near $z=1$, which is consistent with a general theorem for the $r=1$ case derived by Oliensis[9] using $(\phi^3)_6$ field theory. However, if r is not exactly one, as in the case of charm and bottom quarks, our results become $D(z)\sim(1-z)^2$ as we discussed above. The fragmentation function as given by Eq. (23) peaks[10] at $z_{\rm peak}\approx1/(5-5r+r^2)^{1/2}$. For D mesons $z_{\rm peak}\approx0.8$ while for B mesons $z_{\rm peak}\approx0.9$. For T mesons ($t\bar{u}$), $z_{\rm peak}$ appears very close to 1 and the fragmentation function behaves like a delta function.[9]

The analytic expressions for angular distribution of produced mesons can be calculated using the same technique. The result is summarized as

$$\frac{d\sigma}{d\cos\theta}=\frac{\alpha^2\alpha_s{}^2f_M{}^2}{\sin^4\theta_W[(s-M_Z{}^2)^2+\Gamma_Z{}^2M_Z{}^2]s^3m^2}\times\left[\frac{F_p}{(1-r)^2}+(\text{primary}\leftrightarrow\text{secondary})\right] , \tag{24}$$

where F_p is a function which has the general form of

$$F_p=C_0+C_1\cos\theta+C_2\cos^2\theta . \tag{25}$$

The coefficients C_i's are functions of r and couplings V_Q, A_Q, etc. The exact form of F_p will not be presented here because of the lengthy expression; however, the predictions of Eq. (24) will be examined in the next section.

IV. NUMERICAL ESTIMATES

In this section, we present the numerical estimates of (a) total cross section, (b) fragmentation function, (c) angular distribution, and (d) forward-backward asymmetry. As can be seen from Eq. (8), there are several factors for which there are no accurate experimental data. For example, the meson decay constant f_M is not known for all cases we are considering. In our numerical results we used the values

$$\alpha_s=0.2,\ f_M=0.28\ \text{GeV},\ \Gamma_Z=2.9\ \text{GeV} ,$$
$$m_t=40\ \text{GeV},\ m_b=5\ \text{GeV},\ m_c=1.5\ \text{GeV} , \tag{26}$$
$$m_u=0.3\ \text{GeV},\ M_Z=92.9\ \text{GeV},\ \sin^2\theta_W=0.23 .$$

A. Total cross section

For D and B mesons, the total cross section at high c.m. energies ($\sqrt{s}\gtrsim60$ GeV) is given by the analytic result of Eq. (20). The contributions due to the nonzero value of τ^2 (higher-twist mass effects) are not very large and we found these corrections to be about 20—30% (see

Secs. IV B and C). However, for T mesons, τ^2 is no longer small and the contributions from these terms cannot be neglected. Consequently, in this case, all mass terms must be included in the predictions.

The total cross sections for D and B mesons, are predicted by Eq. (20), are shown in Figs. 2(a) and 2(b). At the Z^0 pole, i.e., $\sqrt{s}=92.9$ GeV, the total cross section peaks and increases by approximately two orders of magnitude compared to $\sqrt{s}=60$ GeV. The fact that the cross sections in Figs. 2(a) and 2(b) are not decreasing around $\sqrt{s}=60$ GeV is due to the contributions from Z^0 exchange. This effect should be observable at TRISTAN energies. For lower energies, this contribution becomes smaller as compared to higher-energy cases. Therefore, photon exchange dominates and the cross section decreases as $1/s$. This $1/s$ behavior is also recovered once the energy $\sqrt{s} \gg M_Z$. In Fig. 2(c) we have shown the total cross section of the T meson which includes all mass terms. In this calculation we used the algebraic-manipulation program REDUCE and the Monte Carlo integration routine VEGAS.[11] As we see from Fig. 2(c), at Z^0 pole the $T(t\bar{u})$ meson total cross section is approximately the same order of magnitude as $B(b\bar{u})$ and $D(c\bar{u})$ mesons. Consequently, we expect a large contribution from the T meson in direct hadronic production channels at SLC and LEP.

B. Fragmentation function

Since the fragmentation function is defined by the ratio of two cross sections, i.e., $D(z)\equiv(1/\sigma)d\sigma/dz$, the correc-

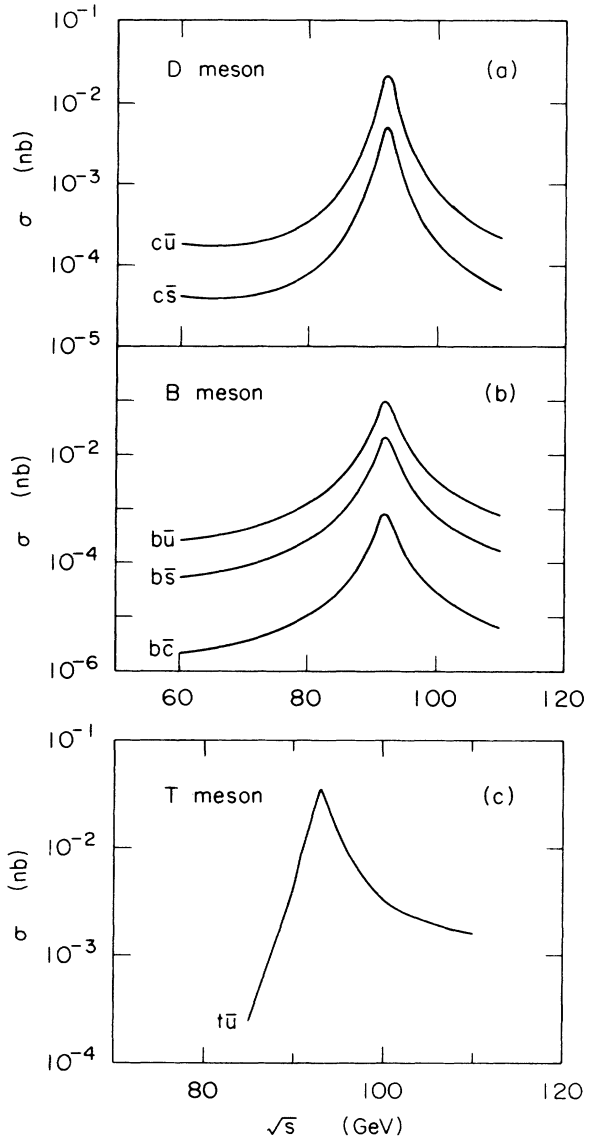

FIG. 2. Total cross sections for inclusive production of (a) D meson, (b) B meson, and (c) T meson.

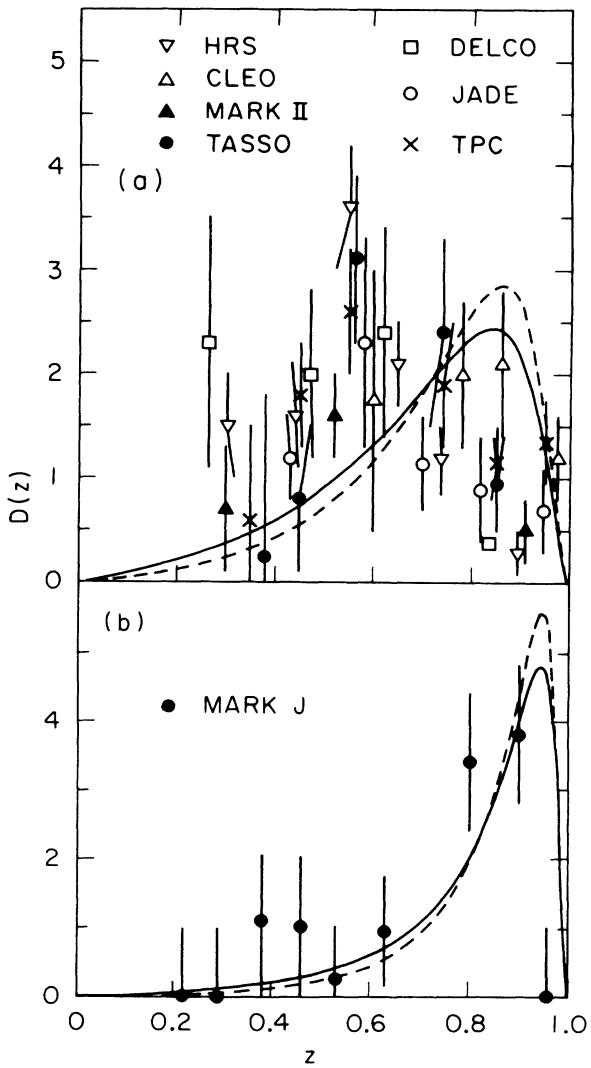

FIG. 3. (a) Charm and (b) bottom fragmentation predictions Eq. (22), compared to various experimental data (Ref. 10). The solid curves in (a) and (b) are pseudoscalar mesons and the dashed curves are vector mesons.

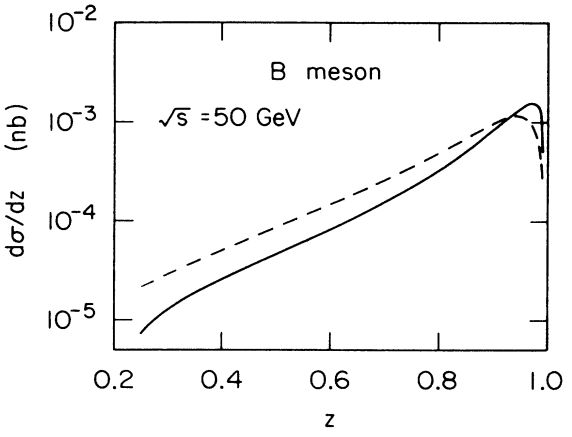

FIG. 4. Differential cross section for B meson at $\sqrt{s}=50$ GeV. The dashed curve is the prediction of Eq. (20) and the solid curve is the numerical estimate which includes higher-twist mass effects.

tions due to higher-twist mass effects are negligible. The leading-twist calculation of fragmentation function was presented in Sec. III where we derived an analytic expression for $D(z)$ given by Eq. (22). As we mentioned in Sec. III, for r close to 1, the fragmentation function is independent of the nature of exchanged particle (i.e., γ, Z^0, or both) and is only a function of z. In Figs. 3(a) and 3(b) we have compared the predictions of Eq. (22) with the experimental data.[12] They are in reasonable agreement with the data for c- and b-quark fragmentation functions. These calculations can be easily extended to vector mesons[5] and the results are shown by dashed curves in Figs. 3(a) and 3(b). For the family of T mesons ($t\bar{u}$, $t\bar{s}$, etc.), the value of r is very close to 1 and due to mass threshold, the expected kinematic range of z for $D_Q^M(z)$ is quite reduced to $z\approx 1$. In fact, to a good approximation, it can be considered as $D_Q^M(z)\sim\delta(z-z_{\text{peak}})$, where z_{peak} is nearly 1.[9]

The differential cross section $d\sigma/dz$ for B mesons is shown in Fig. 4. The solid line represents the calculations with all the mass terms included, while the dashed line is the prediction of the analytic expression (16). From Fig. 4, it is observed that higher-twist mass effects in average account for corrections of approximately 20—30%.

C. Angular distribution

At low energies (e.g., $\sqrt{s}\approx 20$ GeV), the angular distribution of B mesons is expected to have a general form like $a+b\cos^2\theta$. In other words, at these energy ranges the contributions from axial-vector coupling due to Z^0 exchange are negligible and the angular distribution is symmetric. As the energy increases, the axial-vector coupling makes larger contributions and the angular distribution gradually becomes asymmetric and behaves like $A+B\cos\theta+C\cos^2\theta$ [see Eq. (24)]. This property is clearly shown in Figs. 5 and 6 where we have plotted angular distributions of B and T mesons at various c.m. energies. As we see from Fig. 5(a), the angular distribution of B meson at $\sqrt{s}=11$ GeV is almost flat (notice the scale). In fact, near threshold, the process is dominated by two-body exclusive production and the angular distribution is effected by the spin correlations between the two produced mesons. Since we require one of the produced mesons to be a pseudoscalar, the other meson is most likely a pseudoscalar or a vector. Therefore, the net angular distribution, which is a combination[13] of $\sin^2\theta$

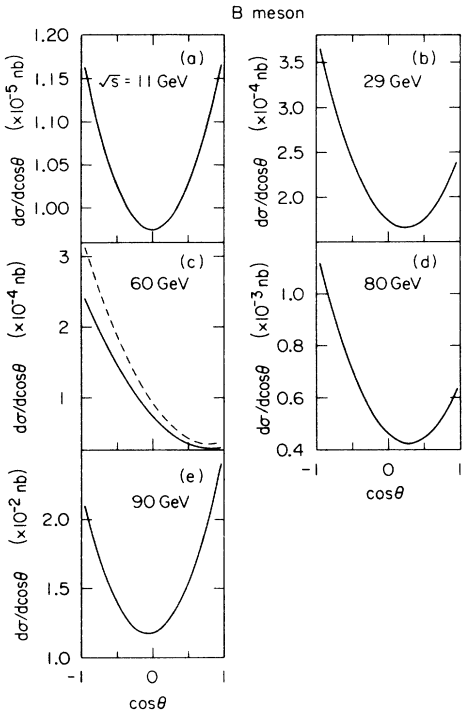

FIG. 5. Angular distribution of B ($b\bar{u}$) meson at (a) $\sqrt{s}=11$ GeV, (b) $\sqrt{s}=29$ GeV, (c) $\sqrt{s}=60$ GeV, (d) $\sqrt{s}=80$ GeV, (e) $\sqrt{s}=90$ GeV. The solid curves in (a), (b), and (c) are the numerical estimates with higher-twist mass effects. The dashed curve in (c) and the solid curves in (d) and (e) are predictions of Eq. (24).

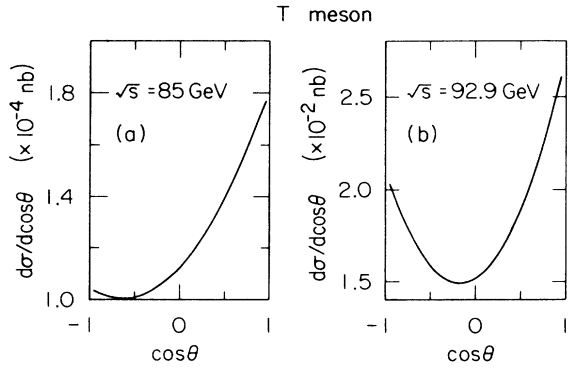

FIG. 6. Angular distribution of T ($t\bar{u}$) meson at (a) $\sqrt{s}=85$ GeV, and (b) $\sqrt{s}=92.9$ GeV with higher-twist mass effects.

(pseudoscalar-pseudoscalar) and $1+\cos^2\theta$ (pseudoscalar-vector), shows very small variation in the entire range of $\cos\theta$. This threshold behavior is also observed for T-meson production as shown in Fig. 6(a). However, as energy increases, angular distributions become more concave because multiparticle channels give larger contributions. This behavior is observed in both Figs. 5 and 6 for B and T mesons, respectively.

D. Forward-backward asymmetry

As we discussed in Sec. IV C the interference between vector and axial-vector currents give rise to asymmetry in angular distributions at high energies. This interference arises from γ and Z^0 cross diagrams or from the product of vector and axial-vector coupling terms in Z^0 diagrams alone. The latter contribution is generally negligible due to the very small magnitude of the vector coupling of Z^0 to leptons. Therefore, the main contribution to the asymmetry is coming from weak-electromagnetic interference terms.

To measure asymmetry, the forward-backward asymmetry A_{FB} is defined as

$$A_{FB}=\frac{1}{\sigma}\left[\int_0^1 \frac{d\sigma}{d\cos\theta}d\cos\theta-\int_{-1}^0 \frac{d\sigma}{d\cos\theta}d\cos\theta\right]. \quad (27)$$

The asymmetries for D, B, and T mesons are shown in Figs. 7 and 8. Since the photon diagram is dominant at low energies, the asymmetry is very small near the threshold of D and B meson production (see Fig. 7). However, for $50 \lesssim \sqrt{s}/\text{GeV} \lesssim 80$, the interference between γ and Z^0 gives a significant contribution to the process. Consequently, at TRISTAN energies, the asymmetry is expected to be large. At the Z^0 pole, the photon contribution is negligible and as a result the asymmetry becomes very small. For higher energies, photon contributions cannot be neglected. In fact, the asymmetry reaches a constant value at asymptotic high energies ($\sqrt{s} \gg M_Z$).

One of the interesting features of Figs. 7 and 8 is the mass effect. Comparing these figures, we note that the

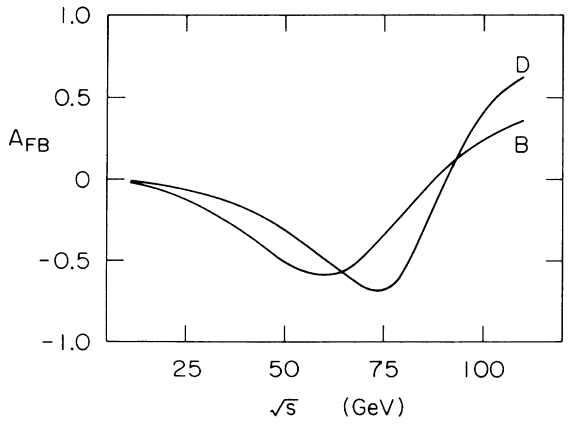

FIG. 7. Forward-backward asymmetry for inclusive D- and B-meson productions.

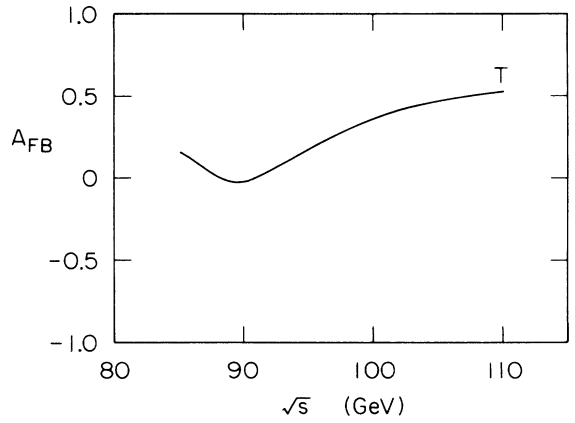

FIG. 8. Forward-backward asymmetry for inclusive T-meson production.

form of the asymmetry of the T mesons around the Z^0 pole is quite different from that of D and B mesons. This is basically due to the large t-quark mass compared to c and b quarks, which causes the higher-twist mass effects to be much more significant for T mesons than D or B mesons. The same behavior can also be observed in the angular distribution of B and T mesons (see Figs. 5 and 6).

V. CONCLUSIONS

In the preceding sections we analyzed the inclusive production of pseudoscalar heavy mesons in e^+e^- annihilation based on a particular model. There are many sources of power-law ($1/Q^2$) corrections[14] to the leading-order perturbative calculation. Our calculation includes one class of such corrections by taking into account higher-order $\tau^2 \equiv 4M^2/s$ terms (higher-twist mass effects). For D and B meson production, the higher-twist mass effects give 20—30% corrections at total c.m. energy of about 60 GeV. Even at $\sqrt{s} \sim 20$ GeV, these corrections are still less than 50%. On the other hand, for T-meson production, these effects are quite significant within the energy range we are considering and must be included in the analysis.

Our predictions for the normalization of the cross sections depend on parameters which are not yet well determined. However, the predictions for fragmentation functions and forward-backward asymmetry are relatively independent of uncertain input parameters. The analytic expression (22) for the heavy-quark fragmentation function gives a reasonable agreement with the experimental data for D and B mesons. The measurement of the forward-backward asymmetry at energies slightly below Z^0 production will provide a good opportunity to test the prediction of higher-twist mass effects in T-meson production, as well as the interference between weak and electromagnetic currents.

Finally, as we mentioned in Sec. II, the underlying mechanism for hadronization of quarks is one of the interesting problems that will be studied at high-energy colliders using heavy-hadron systems. The one-gluon-

exchange mechanism of Ref. 6 which we employed in these calculations is one of the processes that can be tested at those colliders. Once the data become available, then we can see the contributions of higher-order diagrams, or nonperturbative effects to the processes we considered in this study.

ACKNOWLEDGMENTS

We are indebted to Stan Brodsky for suggesting to include weak-electromagnetic interference in this paper and useful discussions throughout this work. We also wish to thank Ben Harms for helpful suggestions at the early stage of this work and Ken Aoki for illuminating conversations. One of us (F.A.) would like to thank SLAC for hospitality during the completion of this project. This work was supported by the Department of Energy, Contract No. DE-AC03-76SF00515.

APPENDIX

A necessary condition for the factorization of the invariant amplitude given by Eq. (1) is that the exchanged gluon momentum is much larger than the QCD scale parameter $\Lambda \sim 100$ MeV. In the exclusive meson and antimeson production process, the momentum transfer is fixed by $(1-r)\sqrt{s}$. However, in the inclusive process, it is not fixed because of the phase-space integration. In this Appendix, we give an estimate to the possible *minimum* momentum carried by the gluon in Fig. 1.

The upper and lower limits of the phase-space integration are given by Eq. (15) in Sec. III. The momentum transferred by the gluon is given by $\sqrt{(1-r)(1-y)s}$ and the nonvanishing contribution comes from the upper limit of y integration. Consequently, the momentum transfer exchanged by the gluon depends on the z variable.

By differentiating the gluon momentum transfer with respect to z, one can obtain the minimum momentum carried by the gluon is given by $2(1-r)M$ (M is the meson mass) at $z=1/(2-r)$. This value becomes larger as the meson mass becomes larger. In the case of D-meson production, $2(1-r)M \sim 600$ MeV which is still larger than $\Lambda \sim 100$ MeV.

---

*Present address: Department of Physics, Brooklyn College, Brooklyn, NY 11210.

†Permanent address: Physics Department, Weber State College, Ogden, UT 84408.

[1]C. Quigg, *Gauge Theories of Strong, Weak, and Electromagnetic Interactions* (Benjamin, New York, 1983).

[2]See *Proceedings of the Stanford Linear Collider User Meeting,* Stanford, California, 1981 (SLAC Report No. 247, 1982).

[3]See *Physics at LEP,* proceedings of the LEP Physics Jamboree, edited by J. Ellis and R. Peccei (CERN Report No. 86-02, 1986).

[4]See *Proceedings of the Second TRISTAN Physics Workshop,* Tsukuba, Japan, 1981, edited by Y. Unno (Report No. KEK 82-1, 1982).

[5]F. Amiri and C. R. Ji, Report No. SLAC-PUB-4023, 1986 (unpublished).

[6]The same model was used for the vector-meson production by L. Clavelli, Phys. Rev. D **26**, 1610 (1982), without including the Z^0-boson contribution.

[7]G. P. Lepage and S. J. Brodsky, Phys. Rev. D **22**, 2157 (1980); S. J. Brodsky and C. R. Ji, Phys. Rev. Lett. **55**, 2257 (1985); F. Amiri, B. C. Harms, and C. R. Ji, Phys. Rev. D **32**, 2982 (1985).

[8]E. L. Berger and D. Jones, Phys. Rev. D **23**, 1521 (1981).

[9]J. Oliensis, Phys. Rev. D **23**, 1430 (1981).

[10]By minimizing the momentum transfer carried by the gluon in Fig. 1 can one derive z_{peak} up to the order of τ^2 as $z_{\text{peak}}=1/(2-r)[1+\tau^2(1-r)]$; see Clavelli, Ref. 6.

[11]G. P. Lepage, J. Comp. Phys. **27**, 192 (1978).

[12]J. Chapman, in *The Sixth Quark,* proceedings of the 12th SLAC Summer Institute on Particle Physics, Stanford, California, 1984, edited by P. M. McDonough (SLAC Report No. 281, 1985); J. Dorfan, in *Proceedings of the 1983 International Symposium on Lepton and Photon Interactions at High Energy,* Ithaca, New York, 1983, edited by D. G. Cassel and D. L. Kreinick (Newman Laboratory of Nuclear Studies, Cornell University, Ithaca, NY, 1983); B. Adeva *et al.*, Phys. Rep. **109**, 121 (1984).

[13]See Brodsky and Ji in Ref. 6.

[14]A. Mueller and P. Nason, Phys. Lett. **157B**, 226 (1985); Nucl. Phys. **B266**, 265 (1986).